# Single M13 bacteriophage tethering and stretching

**Ahmad S. Khalil*, Jorge M. Ferrer†, Ricardo R. Brau†, Stephen T. Kottmann‡, Christopher J. Noren§, Matthew J. Lang*†¶, and Angela M. Belcher†¶‖**

Departments of *Mechanical Engineering, †Biological Engineering, ‡Chemistry, and ‖Materials Science and Engineering, Massachusetts Institute of Technology, Cambridge, MA 02139; and §New England Biolabs, 240 Country Road, Ipswich, MA 01938

Edited by Robert H. Austin, Princeton University, Princeton, NJ, and approved January 12, 2007 (received for review July 8, 2006)

**The ability to present biomolecules on the highly organized structure of M13 filamentous bacteriophage is a unique advantage. Where previously this viral template was shown to direct the orientation and nucleation of nanocrystals and materials, here we apply it in the context of single-molecule (SM) biophysics. Genetically engineered constructs were used to display different reactive species at each of the filament ends and along the major capsid, and the resulting hetero-functional particles were shown to consistently tether microscopic beads in solution. With this system, we report the development of a SM assay based on M13 bacteriophage. We also report the quantitative characterization of the biopolymer's elasticity by using an optical trap with nanometer-scale position resolution. Expanding the fluctuating rod limit of the wormlike chain to incorporate enthalpic polymer stretching yielded a model capable of accurately capturing the full range of extensions. Fits of the force-extension measurements gave a mean persistence length of ≈1,265 nm, lending SM support for a shorter filamentous bacteriophage persistence length than previously thought. Furthermore, a predicted stretching modulus roughly two times that of dsDNA, coupled with the system's linkage versatility and load-bearing capability, makes the M13 template an attractive candidate for use in tethered bead architectures.**

optical tweezers | single molecule | wormlike chain

The Ff class of filamentous bacteriophage, composed of the structurally akin species f1, fd, and M13, has elicited the interest of many wide-ranging scientific communities because of its self-assembling nature. Protected and transported within the highly organized, protein-based capsid is the structural and assembly information necessary for its own production. This structural feature provides a direct and accessible link between phenotype and genotype, which particularly in the case of M13 bacteriophage, has proven advantageous for numerous studies and applications. For instance, combinatorial libraries of polypeptides can be fused to M13 coat proteins, in a technique known as phage display, as a means of screening binding candidates against targets (1). Recently, targets have been extended beyond biologicals to a wide variety of inorganics, in efforts to discover biological systems capable of organizing and growing materials (2). In addition to serving as the vehicle for displaying these ligands, the unique structure of M13 itself has been exploited as a biological template for nanotechnology, such as in the directed synthesis of semiconducting/magnetic nanowires and lithium ion battery electrodes (3–5). Considering its utility as both a genetic blueprint and structural backbone for materials and device architecture, a better understanding of its mechanical behavior and a novel means of actively assembling M13 can greatly advance the design of future M13-based materials.

M13 bacteriophage is a high-production rate virus composed of five different, modifiable proteins, the vast majority of which is major capsid *gene VIII* protein (g8p). Approximately 2,700 copies of this 50-aa monomer encase the virion's ssDNA during assembly in *Escherichia coli*, forming a helical-pitched cylinder that is 7 nm in diameter (6). Joined at one end of the cylindrical particle are typically five copies of small, minor coat g7p and g9p (the remote tip), and at the opposite infective end, five copies of g3p and g6p proteins (the proximal tip). Both end complexes are tightly packaged and contribute little to the WT length of 880–950 nm (7).

Control over the composition and assembly of M13 bacteriophage is not limited to the single-particle level. At critical concentrations and ionic solution strengths, filamentous bacteriophages undergo transitions into various liquid crystalline phases (8), which have subsequently been exploited as macroscale templates for organizing nanocrystals (9). These phase transitions result from purely entropic effects, typically from the competition between rotational and translational entropy (10). Thus, an accurate depiction of M13 elastic properties and degrees of freedom is crucial for phase-transition modeling and prediction.

In the pioneer application of optical trapping to biological systems, Ashkin and Dziedzic (11) lured and manipulated tobacco mosaic virus with laser light, unlocking a flood of subsequent light-based studies of cells, proteins, and single molecules (SMs) (12, 13). To our knowledge, the efforts to optically trap and study single viruses have not continued with the same rigor of, for instance, DNA. Nevertheless, these efforts could provide interesting, new platforms for SM biophysics, which remains heavily reliant on a few accessible assays, such as the gliding filament, the tethered bacterium, and the tethered bead (14). In this article, we merge advances in genetic engineering of M13 capsids with instrumentation to unlock a SM tool. Additionally, we demonstrate that M13 can be a strong and versatile biopolymer alternative to dsDNA in constructing the instrumental tethered bead assay.

The developed M13-based assay also provides a means of investigating unknown and contentious filamentous bacteriophage mechanical properties. Recently, an investigation into the interaction of colloidal microspheres in bacteriophage "rod" suspensions cast doubt over previously accepted persistance length values (15). Specifically, deviations between depletion attraction measurements and "rigid-rod" theories were resolved when rod flexibility was introduced in the model. From this analysis, persistence lengths two to three times smaller than 2.2 $\mu$m, the commonly cited value obtained from dynamic light scattering of bacteriophage solutions, were suggested (16). Furthermore, spontaneous nano-ring formation was readily observed when M13 remote and proximal tips were functionalized with hexahistidines ($H_6$) and divalent cations, respectively (17). Even without modification, intricate circular structures were assembled from M13 films on thin polymer multilayers (18).

In this article, we first demonstrate a robust and tunable method for generating M13 tethers in solution. Next, we inves-

Author contributions: A.S.K., J.M.F., R.R.B., M.J.L., and A.M.B. designed research; A.S.K., J.M.F., and S.T.K. performed research; A.S.K., J.M.F., and C.J.N. contributed new reagents/analytic tools; A.S.K., J.M.F., and R.R.B. analyzed data; A.S.K. wrote the paper; and M.J.L. and A.M.B. advised/oversaw research and edited the manuscript.

The authors declare no conflict of interest.

This article is a PNAS direct submission.

Abbreviations: SM, single molecule; WLC, wormlike chain; *F-x*, force-extension.

¶To whom correspondence may be addressed. E-mail: mjlang@mit.edu or belcher@mit.edu.

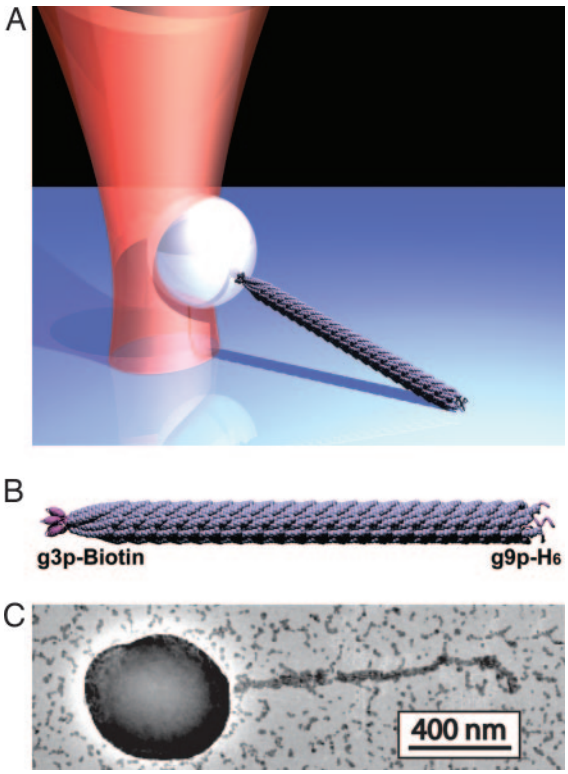


**Fig. 1.** Single M13 bacteriophage stretching and modification. (*A*) Rendering of M13 bacteriophage stretching by an optical trap (not to scale). (*B*) Major capsid g8p monomers form an ordered helical shell that encases its ssDNA. The g8p coat was reconstructed from x-ray fiber crystallographic data (Protein Data Bank ID code 1ifj). The end complexes (identified in purple) consist of several copies of genetically modifiable g9p and g3p monomers. In *B*-$H_6$ phages, $H_6$ tags were fused to g9p via plasmids inserted into bacterial hosts. Each copy of g3p was biotinylated after encoding for a selenopeptide fusion directly into M13's *gene III* (not to scale). (*C*) A transmission electron microscopic image of the assembly architecture, where a gold-binding peptide was fused to g8p monomers for gold nanoparticle incorporation along the length of the capsid (note that bead is larger than beads used for stretching).

tigate the SM elasticity via optical tweezers stretching and modify the appropriate limit of the wormlike chain (WLC) model to accurately capture force-extension (*F-x*) measurements. Finally, we discuss significant features and extensions of this system.

## Results

**Tethering.** Once the genetic constructs encoding for modified forms of specific capsid proteins were engineered, phages expressing the desired polypeptide sequences were readily amplified in bacterial hosts. For the majority of our stretching measurements, we designed heterobifunctional phages (termed *B*-$H_6$), displaying $H_6$ epitopes at remote tips and biotin molecules linked through selenocysteine (Sec) residues at proximal tips. Guided by the established protocols for SM dsDNA studies (19), a procedure for suspending *B*-$H_6$ phage in solution between antibody-functionalized coverslips and streptavidin-coated polystyrene microspheres was developed (Fig. 1). This procedure was robust and repeatable, generating ≈20–40 tethered beads and minimal nonspecifically immobilized beads per visual field of view (110 $\mu$m × 110 $\mu$m).

The M13 genome provides a convenient platform for displaying and interchanging functional groups at M13 tips and the major capsid. We designed three variant genetic constructs and tested them in the developed assay. In each, biotin molecules at proximal tips were replaced with short *S*1 peptides (WDPY-SHUQHPQ) carrying the HPQ motif, which is known to bind streptavidin with micromolar affinity (20). The first construct (*S*1-$H_6$) yielded analogous arrays of tethered beads, possessing surprisingly high stability and strength (as demonstrated below). To the *S*1-$H_6$ genome, peptide markers were additionally cloned upstream of the g8p N terminus to give two different heterotrifunctional phages. The first, *S*1–9-$H_6$, was endowed with a known gold-binding octamer (VSGSSPDS) on each copy of g8p, such that nanoparticle-mineralized capsids were observed after incubation with 5-nm gold colloidal solution (Fig. 1*C*) (21). As illustrated in the transmission electron microscopic image of Fig. 1*C*, there is a single mode of assembly, where only the proximal tip is adapted to bind beads. The second trifunctional construct, *S*1-*E*4-$H_6$, was designed to present negatively charged tetraglutamate species (AEEEEPDA) at each g8p N terminus. The localized negative charge coordinates divalent cation and certain inorganic material precursors, and, in particular, has been shown to nucleate single crystal $Co_3O_4$ nanowires (5). Following identical procedures, this construct analogously tethered beads in solution. In essence, the location and moiety to which the M13 construct binds is tunable, extending even to inorganic materials.

**Stretching.** The elastic properties of M13 are critical to its use as a SM tool, nanotechnology assembly vehicle, or liquid crystal building block. In an effort to characterize them, single M13 molecules were stretched with a high-resolution optical trap using procedures similar to those of ref. 22 for short dsDNA tethers (see *Materials and Methods*). Briefly, 440-nm-diameter polystyrene beads, affixed to proximal ends of M13, were trapped by the optical gradient forces of a tightly focused laser beam and positioned a set height above the coverslip surface. The piezo-electric stage was then translated laterally while bead displacements from the trap center were recorded, and, with the necessary calibrations (12), these results were converted to *F-x* measurements.

Stage-based stretching of M13 molecules with optical trap stiffness in the range of 0.25–0.35 pN/nm gave *F-x* measurements from fractions of a pN up to 30–40 pN. Despite its hierarchical structure, M13 *F-x* behavior was reminiscent of typical WLC biopolymer stretching (Figs. 2 and 3). In fact, plotted alongside a typical *F-x* curve for a 3,500-bp dsDNA molecule, stretched by identical procedures, the M13 response appeared very similar to that of dsDNA, albeit much stiffer (Fig. 2). After a small entropic elasticity regime, the thermal random-walk fluctuations governing the filament's orientation were stifled and its end-to-end distance approached its contour length, or the B-form length in the case of dsDNA. Just before the molecule reached its contour length it began to display compliance, and enthalpic stretching, or simply linear elasticity, accounts for actual polymer extension.

While more work is needed to properly characterize and identify where M13's enthalpic stretching regime breaks down, a preliminary investigation at higher forces showed that M13 experiences no abrupt overstretching transitions, as does dsDNA at 60–65 pN (Fig. 3*A*) (23). In all instances, the *F-x* response was reversible and showed no plasticity, permanent deformation, or even force plateau through loads of 70 pN, the maximum achievable force given our experimental conditions, namely where the trap's linearity remained trustworthy. Higher forces were attained by increasing the laser power delivered to the specimen and, in some cases, substituting larger beads (984 nm diameter) in place of 440-nm beads to increase the instrument's potential force generation.

**Modeling.** The mechanical properties and fluctuations of semiflexible polymers are well described by the WLC (24). Here, the configuration of a polymer is represented by a space curve of fixed, zero tension contour length, $L_0$, with a bending energy that

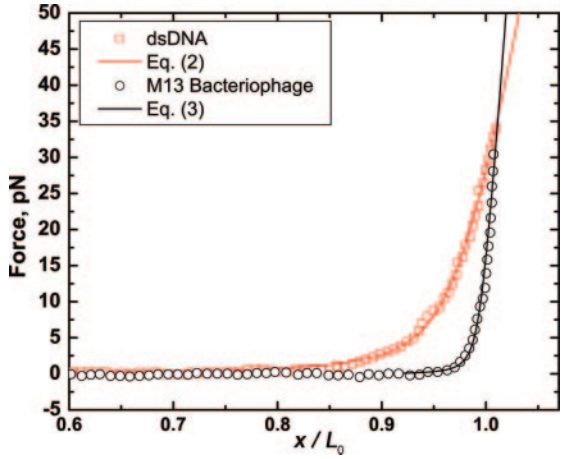


**Fig. 2.** *F-x* comparison of M13 bacteriophage and dsDNA. A typical *F-x* measurement for M13 bacteriophage (○) with corresponding fit, using Eq. **3**, overlaid on the data. A modified form of the WLC's fluctuating rod limit was developed to describe the full range of extensions. The M13 behavior is suggestive of a stiffer analog to dsDNA, for which a typical *F-x* measurement (□) is plotted along with its corresponding fit to the modified Marko-Siggia form of Eq. **2**. Average DNA parameters, $l_p = 42.1 \pm 2.9$ nm, $K = 1{,}016.0 \pm 180.2$ nm, and $L_0 = 1{,}185.7 \pm 19.4$ nm, extracted from a set of five independent molecules agree well with previous literature values and theoretical 3,500-bp contour length, validating our experimental stretching procedures.

is quadratic in the chain curvature. External forces stretching WLC polymers, therefore, do work against the conformational entropy of the chain (25). With space curve, $\mathbf{r}(s)$, parameterized by the polymer's arc length $s$, the chain's curvature is simply $\kappa = |\partial^2\mathbf{r}(s)/\partial s^2| = |\partial\hat{\mathbf{t}}(s)/\partial s|$, where $\hat{\mathbf{t}}(s)$ is the unit vector tangent to the chain. The resulting elastic energy, $E$, of a WLC polymer being mechanically stretched by a uniaxial force is:

$$\frac{E}{k_BT} = \int_0^L \frac{l_p}{2} k^2\, ds - \frac{F}{k_BT} x\,, \qquad [1]$$

where $x$ is the total extension of the chain, $l_p$ the persistence length, $k_B$ the Boltzmann constant, $T$ the absolute temperature, and $F$ the force. The persistence length is the characteristic length scale over which thermal fluctuations begin to dominate the orientation of the chain's tangent vectors.

Using a statistical mechanical treatment of the WLC, the equilibrium extension and other relevant thermodynamic variables were evaluated from the Boltzmann distribution $e^{-E/k_BT}$. In the long polymer limit, Marko and Siggia (25) derived an interpolation formula that has been widely used to model stretching data, such as that of dsDNA (26). The modified Marko-Siggia form,

$$F = \frac{k_BT}{l_p}\left[\frac{1}{4(1 - x/L_0 + F/K)^2} - \frac{1}{4} + \frac{x}{L_0} - \frac{F}{K}\right], \qquad [2]$$

accounts for enthalpic elongation and was used to capture a broader range of extensions, ultimately predicting dsDNA persistence lengths of 40–50 nm and elastic stretching modulus, $K$, of 1,000–1,100 pN (22). As indicated above, we validated our experimental methods by stretching 3,500-bp dsDNA using identical procedures to those of M13 phage. A small data set ($n = 5$) of *F-x* measurements was generated and fit to Eq. **2**. The resulting parameters, $l_p = 42.1 \pm 2.9$ nm, $K = 1{,}016.0 \pm 180.2$ pN, and $L_0 = 1{,}185.7 \pm 19.4$ nm, agreed well with previous

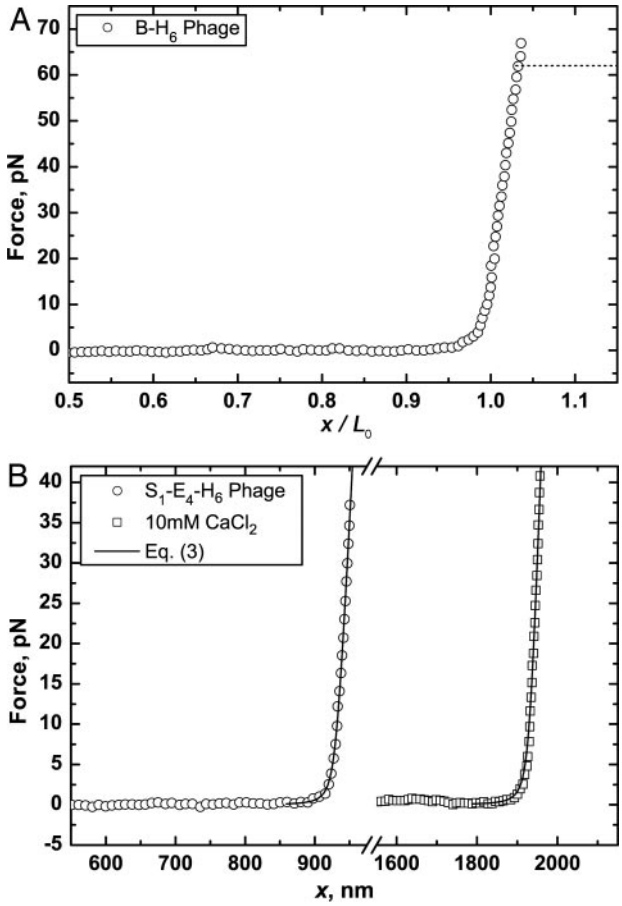


**Fig. 3.** Mechanical features and extensions of the M13 system. (*A*) The *F-x* behavior of M13 loaded up to 70 pN is fully elastic, exhibiting no transitions or permanent deformation, unlike that of dsDNA, which exhibits an abrupt force plateau at 60–65 pN (dashed line) to an ''overstretched'' form. (*B*) When modified to display streptavidin-binding *S1* peptides on g3p and tetraglutamate peptides on g8p, the mechanics of the *S1-E4-H6* variant remained robust and comparable to that of *B-H6* phage. Interestingly, the tethered system remained intact for relatively large loads because M13 expresses multiple copies of the linking peptides at each filament end. In the presence of 10 mM $CaCl_2$, negatively charged *S1-E4-H6* phage was induced to form lateral bundles, which were manifested as much longer tethers in their *F-x* measurements.

predictions and the theoretical contour length of 1,183 nm (using 0.338 nm/bp), thus confirming our procedures.

The thermodynamic limit of $L_0 \gg l_p$ is not valid for filamentous bacteriophage, thus Eq. **2** is inapplicable for describing its mechanics. Instead, the WLC must be solved with the appropriate boundary conditions to account for finite-length effects. In general, this is a difficult task; however, an analytical solution exists for the equilibrium extension of polymers with contour length of the order of, or shorter than, persistence length ($L_0 \leq 2l_p$). In this fluctuating rod limit, thermal undulations in the chain appear increasingly smoothed out as compared with random-walk polymers (27). With tangent vectors making only small deviations away from the direction of the force, a harmonic approximation can be taken and the generating functional method used to obtain the average extension (28).

Inspired by the approach of Odijk (29), we have modified this solution to include a stretching term that allows us to model the full range of bacteriophage extensions. An effective stretching energy that is quadratic in the polymer's elongation, $E_e = \int_0^L \frac{1}{2}K(s/s_0 - 1)^2 ds$, was added to Eq. **1**. In the case of small elongations, the resulting average extension is:

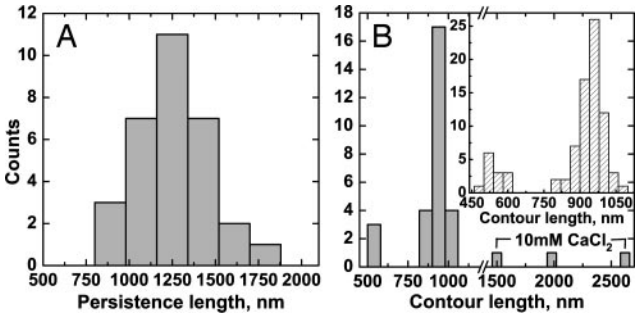


**Fig. 4.** Histogram results for $l_p$ and $L_0$ for the complete set of 31 independent M13 bacteriophage specimens. (*A*) Persistence lengths centered about an average value of 1,265.7 ± 220.4 nm. (*B*) Contour length values, under standard experimental conditions, revealed dual length populations, with averages 939.7 ± 46.1 nm and 532.0 ± 20.5 nm, corresponding to full and shorter plasmid-packaging lengths, respectively. Occurrences of longer M13 bundles were observed in the presence of 10 mM $CaCl_2$. (*Inset*) Contour length distributions estimated from high-resolution atomic force microscopic images of 83 different bacteriophage specimens confirmed the stretching-predicted lengths ($L_0$ = 945.4 ± 51.8 nm and 542.3 ± 39.1 nm).

$$x = L_0 - \frac{k_B T}{2F}\left[ L_0\sqrt{\frac{F}{A}}\coth\left(L_0\sqrt{\frac{F}{A}}\right) - 1\right] + \frac{FL_0}{K}, \qquad [3]$$

where $A = l_p k_B T$ and $K$ is an elastic stretching modulus (28, 30). Here, the end tangent vectors are assumed to be collinear with the force, consistent with our experimental setup, where linkages were engineered from the proximal and remote tips (i.e., from small, pivoting proteins as opposed to the crystalline g8p shell).

A typical fit of a single M13 *F-x* measurement to Eq. **3** is shown in Fig. 2, where it is evident that the full range of extensions is generally well described by the modified model. In all, stretching curves for 31 different specimens were obtained and fit, and the resulting parameters then averaged to ultimately obtain $l_p$ = 1,265.7 ± 220.4 nm, two contour lengths $L_0$ = 939.7 ± 46.1 nm and 532.0 ± 20.5 nm, and $K$ = 2176.2 ± 656.3 pN. The full results for $l_p$ and $L_0$ are pictorially collected in the histograms of Fig. 4, where the dual contour length population can undoubtedly be observed. These two lengths corresponded to bacteriophage packaging full M13 genomes and shorter g9p-$H_6$ plasmids (see *Materials and Methods*) (1). The relative frequency of full genome- to plasmid-packaging phages depends on various preparation factors, and the histogram results are not reflective of the true relative populations, particularly because we focused our stretching studies on full-length particles. The corresponding lengths, on the contrary, accurately depict how phage length scales with the number of nucleotide bases in the packaged DNA: 7,222 in full M13KE vectors and 3,957 in $H_6$ plasmids.

Average M13 contour lengths are commonly reported between 880 and 950 nm (1, 31). To more precisely assess our model-predicted contour lengths, atomic force microscopic images were taken of the same *B*-$H_6$ sample used for stretching. The contour lengths of 83 different bacteriophages were measured by using manual image processing techniques from 10 phase images (5 $\mu$m × 5 $\mu$m or 3 $\mu$m × 3 $\mu$m). The distribution (shown in Fig. 4*B Inset*) confirms the existence of dual length populations, and the average values of 945.4 ± 51.8 nm and 542.3 ± 39.1 nm corresponded well with the values obtained from stretching data.

**Features and Extensions of the System.** Variant M13 constructs, *S*1-$H_6$, *S*1–9-$H_6$, and *S*1-*E*4-$H_6$, readily tethered beads in solution when integrated into our SM assay. Force-based studies with these variants elucidated some further, interesting features of the overall system and provided a means of exploring genetically coupled mechanics.

Stretching of *S*1-*E*4-$H_6$ revealed, first, that tethers were capable of withstanding respectable forces, of at least 40 pN, despite the use of relatively low affinity interactions with streptavidin beads (Fig. 3*B*). This unique strength can be attributed to the multiple copies of g3p being displayed on the proximal tip of the capsid. As a result, the roughly five attachment points between *S*1 and streptavidin are, most likely, sharing the total load and providing an aggregate strength greater than that of the weaker individual bonds. The linkages in *B*-$H_6$ tethers, therefore, are likely to withstand much higher forces than those needed to dissociate single biotin–streptavidin or $H_6$–antibody bonds.

The second result answers the question of what effect an engineered modification in the major coat g8p may have on the filament's mechanics. Preliminary results suggest that *S*1-*E*4-$H_6$ phage exhibits comparable mechanical properties to those of *B*-$H_6$, despite having highly charged tetraglutamate species along its filamentous capsid. Indeed, a set of four full-length *S*1-*E*4-$H_6$ phages yielded an average $l_p$ of 1,250.6 ± 164.2 nm, $L_0$ of 931.6 ± 26.7 nm, and $K$ of 1,796.9 ± 367.9 pN.

Because of their polyelectrolyte nature, M13 and other filamentous bacteriophage can be induced to laterally aggregate into bundles by metal divalent cations (32). The additional negative charge built into *S*1-*E*4-$H_6$ is advantageous in spurring this phenomenon at lower divalent cation concentrations than typically required (40–80 mM $Ca^{2+}$). So, we tested whether *S*1-*E*4-$H_6$ bundles, generated in the presence of a small amount of $Ca^{2+}$, could also be incorporated into our tethering assay. *S*1-*E*4-$H_6$ phage was incubated in 10 mM $CaCl_2$ for 30 min and then introduced into flow cells with streptavidin-coated beads. While certainly not as prevalent as single M13 tethers, there was indeed evidence of tethered bacteriophage bundles. For instance, Fig. 3*B* illustrates the stretching of one of three long bundles. The corresponding contour lengths of the three specimens, included in the histogram of Fig. 4*B*, significantly exceeded those of single bacteriophage and therefore could not have corresponded to single particles. It should be noted that additional work is still needed to fully characterize these bundles, such as to test the effect of varying cation concentration on bundle sizes and mechanics.

## Discussion

A significant challenge in SM biophysics research is in developing creative and trustworthy assays to link the biological problem of interest to the high-resolution instruments responsible for detection and manipulation. To address this challenge, we have harnessed a robust protein-based template that possesses the genetic advantages typically reserved for DNA. In particular, M13 bacteriophage provides direct genotypic control over the molecules displayed on it, and, because of its hierarchical structure, these molecules can be targeted to specific locations on the polymer. This feature of excellent physical handle connectivity is advantageous for two reasons. First, versatility is embedded into the system by virtue of the widely studied and modifiable M13 genome. M13KE, a derivative of the M13 genome with cloning sites introduced for fusion to *gene III* (New England Biolabs, Ipswich, MA), and various phagemid vectors are commercially available. With these, reactive peptide epitopes, including the $H_6$ tag, the HA tag, and cysteine residues, as well as proteins can be fused to g3p, g9p, or g8p (17, 21, 33). Modes of attachment can, as a result, be diversified, potentially allowing for SM handling of biological species previously unsuited for DNA tethering, such as transcription factors. Furthermore, the displayed molecules need not be solely vehicles for attachment but can also be the species of study. For instance, mechanically interesting proteins, such as dimeric streptavidin, have been successfully expressed on M13 g3p (34). Conceivably,

the M13 template can be made to carry the protein of interest and simultaneously serve as the mechanical tether. Second, in tethered bead assays, binding is restricted to M13 ends, ensuring that tethers of finite length are always generated and that force corrections, because of ill-defined geometries, are small. In experiments with protein biopolymers, such as F-actin, often the strategy is to unselectively biotinylate monomers and hope the desired attachment architecture is obtained in solution. As a consequence, beads tend to bind numerous locations along the filaments, resulting in filament wrapping and unwanted bending contributions during stretching (35).

The M13 system appears well suited for higher force studies, such as for protein extension and distortion, particularly now that the force capability of optical tweezers is increasing (36). In contrast to dsDNA, phage showed no deviation from standard entropic/enthalpic stretching when subjected to loads through 70 pN. Nonetheless, in optical tweezers-based studies, dsDNA is commonly used to translate forces to a protein of interest (37). The M13 template may be better able to communicate these forces because it is stiffer (longer $l_p$ and higher $K$) than DNA. Furthermore, the M13 template can provide multiple, localized attachments to the species of interest to prevent or delay detachment.

Characterizing filamentous bacteriophage mechanics and flexibility has been a scientific challenge. Thus far, literature values for $l_p$ have been wide-ranging, though a rigorous investigation since the dynamic light scattering studies of fd and M13 suspensions from >15 years ago has been lacking. The often cited value, $l_p = 2.2$ $\mu$m, was derived from fitting fluctuations in scattering intensity to theoretical models for Brownian dynamics that are built on various other models, assumptions, and correction factors (38). These fits highly depend on hydrodynamic and structural parameters and are therefore associated with large variances (31). Furthermore, $l_p$ estimates from electron microscopy images (880 nm–6 $\mu$m) are subject to sample preparation artifacts yet have been widely used as standards by which to confirm dynamic light scattering results (31). In fact, dynamic light scattering has been known to give a broad range of predictions for other semiflexible polymers, including F-actin (39); thus, continuing efforts to reconcile and validate the different techniques are critical.

In this article, the characterization of the SM elasticity of filamentous bacteriophage was presented. The fluctuating rod limit of the WLC was equipped with an elastic chain stretching term and then used to model optical tweezers stretching data. The extracted mean $l_p$ (1,265 nm) supports recent predictions that filamentous bacteriophage $l_p$ may be shorter than previously thought (16). Additionally, the two expected contour lengths (at full length and g9p-$H_6$ plasmid length) and a mean $K$ near 2,200 pN, approximately double that of dsDNA, were obtained. It should be noted that although the model described $F$-$x$ measurements well it may not have captured all of the polymer's complex mechanical behavior. For instance, M13 is a chiral molecule and may also undergo stretching-coupled twisting (40). It should also be noted that for finite-length molecules experimental conditions must reflect the desired statistical ensemble, as different ensembles cannot be assumed equivalent (30). Stage-based stretching, as implemented here, applies a nearly constant force at each increment, consistent with the model's assumed ensemble. In fact, under our experimental conditions, it can be shown that the M13 polymer is in equilibrium. For instance, at trap stiffness lower than that used for stretching, M13 relaxation time was estimated at 0.32–0.37 ms by the autocorrelation of bead position at $x/L_0 = 0.72$–$0.92$, negligibly longer than the corresponding time for untethered beads, 0.30 ms.

Biopolymer mechanics are intrinsically related to biological function. Microtubules, with mm-long $l_p$, provide cellular rigidity and structure, actin is responsible for cell motility, while DNA, with short $l_p$, is easily folded and packaged into chromosomes. Filamentous bacteriophage capsids have the dual responsibility of safeguarding viral DNA as well as locating and binding host receptors during infection. As a result, they are robust, yet adaptable, structures. We anticipate that the techniques developed for M13 bacteriophage will provide a broadly applicable tool for facilitating future SM studies and furthering biopolymer modeling and mechanics.

## Materials and Methods

**Genetic Engineering of Capsid Proteins.** Controlled modification of all M13 capsid proteins is possible. To the N terminus of each g3p, a short Sec-containing peptide (SARVXHGP, where X is Sec) was fused by cloning directly into the M13 genome (M13KE) and amplifying in the presence of 2 $\mu$M sodium selenite (*Sec1*) (33). Compared with cysteine ($pK_a = 8.1$), Sec has a $pK_a$ of 5.2 and thus can be targeted for nucleophilic substitution at acidic pH.

Cloning directly into the M13 genome is not as straightforward for g9p modification because of overlapping genes. Therefore, we PCR-amplified a primer encoding for $H_6$ upstream of the M13 virus *gene IX*. This extended *gene IX* was cloned into a pAK-derived phagemid, separate from the full M13 genome, such that the fusion protein was under *lac* promoter control (3, 17). As a result, bacterial hosts harboring this plasmid were induced to express the fusion protein with 1 mM isopropyl $\beta$-D-thiogalactopyranoside. Upon infection with helper phage (*Sec1*), hetero-bifunctional particles (*Sec1*-$H_6$), packaging either full M13KE genomes or recombinant plasmids, were produced.

Once the desired genetic constructs were designed, phages were amplified in bacterial hosts and then purified by PEG-NaCl precipitation. Sec residues fused to g3p were subsequently biotinylated with 1 mM iodoacetyl-$PEO_2$-biotin (Pierce, Rockford, IL) in 30 mM acetate buffer (pH 5), yielding the final phage species, $B$-$H_6$.

**Instrument Design.** Phage stretching was performed in an optical trap setup constructed around an inverted microscope (Nikon, Tokyo, Japan) as described (41). Briefly, a high numerical aperture objective (×100, 1.40 N.A.; Nikon) tightly focuses a 1,064-nm laser (Coherent, Santa Clara, CA) to form the optical trap. The trap location at the specimen plane was computer-controlled by a pair of orthogonally oriented acousto-optic deflectors (Intra-Action, Bellwood, IL), and the positioning of the specimen was manipulated with a nanometer-resolution piezo-electric stage (Polytec PI, Auburn, MA). The combination of a 975-nm laser (Corning, Corning, NY) and a position-sensitive device (Pacific Silicon, Westlake Village, CA) was used for back-focal plane position detection as collected from bead scattering (42). Data were acquired with an A-D board (National Instruments, Austin, TX), and custom software (LabView, National Instruments) was developed to automate experimental runs and data acquisition. Data analysis was performed with software written in MATLAB (Mathworks, Natick, MA).

**Single M13 Stretching.** A procedure for suspending M13 phages between surface and polystyrene microspheres was developed. Penta-His antibody (20 $\mu$g/ml; Qiagen, Valencia, CA) in TBS buffer (100 mM Tris·HCl/150 mM NaCl, pH 7.5) was incubated in 10 $\mu$l of flow cells, constructed from glass slides and etched coverslips. After washing flow cells with 200 $\mu$l of 3 mg/ml Casein (Sigma, St. Louis, MO) in TBS, 40 $\mu$l of $10^8$ to $10^9$ $B$-$H_6$ phages per microliter was flowed in and allowed to bind the antibody-coated coverslip surface for 25 min at room temperature. After another washing step with 100 $\mu$l of 0.15 mg/ml Casein solution, 40 $\mu$l of a 60 pM concentration of 440-nm streptavidin polystyrene microspheres (Spherotech, Lake Forest, IL) was exposed to immobilized phages for 20 min. Flow cells were finally washed with 200 $\mu$l of TBS.

Stretching candidates were located by visual inspection. Tethered beads were then optically trapped and subjected to a lateral centering routine. Next, the vertical height of the trap center was determined and fixed such that beads were offset 150–200 nm from the surface. Stretching was performed by repeatedly stepping the stage every 50 ms in increments of 10 nm while voltage samples from the position-sensitive device, acquired at 5 kHz, were averaged to obtain the bead position at each "fixed force" step. Beads from each stretching experiment were position-calibrated by using procedures to map position-sensitive device voltage readings to spatial bead displacements (43). Trap stiffness was determined from the positional variance of beads and the Stokes drag method (12).

Output voltage, stage position, position calibration, and trap stiffness data were compiled to generate corresponding *F-x* measurements. Furthermore, the correct force and extension components were computed by using the appropriate geometric corrections as described (22).

**DNA Stretching.** Preparation of DNA flow cells followed from the wealth of published protocols. Briefly, flow cell bottom surfaces were coated with 20 $\mu$M anti-digoxigenin polyclonal antibody (Roche Applied Science, Indianapolis, IN) for 45 min and subsequently washed with 200 $\mu$l of 3 mg/ml Casein in PBT (100 mM phosphate buffer/0.1% Tween 20, pH 7.5). A 20 pM concentration of 3,500-bp dsDNA (Oligo 1, [Biotin]-5′-AAT CCG CTT TGC TTC TGA CT-3′; Oligo 2, [Digoxigenin]-5′-TTG AAA TAC CGA CCG TGT GA-3′), which was PCR-amplified in TE buffer (10 mM Tris/1 mM EDTA, pH 7.5), was incubated with a 60 pM concentration of 440-nm streptavidin microspheres for 4 h at 4°C and then exposed to the antibody-functionalized flow cells. Finally, the flow cells were washed with 400 $\mu$l of 0.15 mg/ml Casein. DNA stretching procedures were analogous to those of M13.

**Imaging.** Transmission electron microscopy images were collected with a 2010 microscope (JEOL, Tokyo, Japan), operating at 200 kV. Atomic force microscopic images were carried out with a Nanoscope IV (Digital Instruments, Sterling Heights, MI) operating in tapping mode under ambient conditions using etched silicon cantilever tips.

We thank A. Prasad for helpful discussions and an anonymous reviewer for modeling suggestions. Financial support was provided by the Army Research Office Institute of Collaborative Biotechnologies, the David and Lucile Packard Foundation, the Massachusetts Institute of Technology/ National Institute of General Medical Sciences Biotechnology Training Program (R.R.B.), and startup funds from the Department of Mechanical and Biological Engineering at the Massachusetts Institute of Technology (M.J.L.).

1. Webster R (2001) in *Phage Display: A Laboratory Manual*, eds Barbas CF, Burton DR, Scott JK, Silverman GJ (Cold Spring Harbor Lab Press, Cold Spring, NY), pp 1.1–1.37.
2. Whaley SR, English DS, Hu EL, Barbara PF, Belcher AM (2000) *Nature* 405:665–668.
3. Mao C, Flynn CE, Hayhurst A, Sweeney R, Qi J, Georgiou G, Iverson B, Belcher AM (2003) *Proc Natl Acad Sci USA* 100:6946–6951.
4. Mao C, Solis DJ, Reiss BD, Kottman ST, Sweeney RY, Hayhurst A, Georgiou G, Iverson B, Belcher AM (2004) *Science* 303:213–217.
5. Nam KT, Kim D-W, Yoo PJ, Chiang C-Y, Meethon N, Hammond PT, Chiang Y-M, Belcher AM (2006) *Science* 312:885–888.
6. Opella AJ, Stewart PL, Valentine KG (1987) *Q Rev Biophys* 19:7–49.
7. Newman J, Swinney HL, Day LA (1977) *J Mol Biol* 116:593–606.
8. Adams M, Dogic Z, Keller SL, Fraden S (1998) *Nature* 393:349–352.
9. Lee S-W, Mao C, Flynn CE, Belcher AM (2002) *Science* 296:892–895.
10. Onsager L (1949) *Ann NY Acad Sci* 51:627–659.
11. Ashkin A, Dziedzic JM (1987) *Science* 235:1517–1520.
12. Svoboda K, Block SM (1994) *Annu Rev Biophys Biomol Struct* 23:247–285.
13. Mehta AD, Rief M, Spudich JA, Smith DA, Simmons RM (1999) *Science* 283:1689–1695.
14. Block SM (1997) *Nature* 386:217–219.
15. Lin K-H, Crocker JC, Zeri AC, Yodh AG (2001) *Phys Rev Lett* 87:088301.
16. Lau AWC, Lin K-H, Yodh AG (2002) *Phys Rev E* 66:020401.
17. Nam KT, Peelle BR, Lee S-W, Belcher AM (2004) *Nano Lett* 4:23–27.
18. Yoo PJ, Nam KT, Qi J, Lee S-K, Park J, Belcher AM, Hammond PT (2006) *Nat Mater* 5:234–240.
19. Lang MJ, Fordyce PM, Engh AM, Neuman KC, Block SM (2004) *Nat Methods* 1:133–139.
20. Schmidt TGM, Koepke J, Frank R, Skerra A (1996) *J Mol Biol* 255:753–766.
21. Huang Y, Chiang C-Y, Lee SK, Gao Y, Hu EL, Yoreo JE, Belcher AM (2005) *Nano Lett* 5:1429–1434.
22. Wang MD, Yin H, Landick R, Gelles J, Block SM (1997) *Biophys J* 72:1335–1346.
23. Smith SB, Cui Y, Bustamante C (1996) *Science* 271:795–799.
24. Kratky O, Porod G (1949) *Rec Trav Chim* 68:1106–1123.
25. Marko J, Siggia ED (1995) *Macromolecules* 28:8759–8770.
26. Smith SB, Finzi L, Bustamante C (1992) *Science* 258:1122–1126.
27. Wilhelm J, Frey E (1996) *Phys Rev Lett* 77:2581–2584.
28. Hori Y, Prasad A, Kondev J (2007) *Phys Rev E*, in press.
29. Odijk T (1995) *Macromolecules* 28:7016–7018.
30. Keller D, Swigon D, Bustamante C (2003) *Biophys J* 84:733–738.
31. Beck K, Duenki RM (1990) *J Struct Biol* 105:22–27.
32. Tang JX, Janmey PA, Lyubartsev A, Nordenskiöld L (2002) *Biophys J* 83:566–581.
33. Sandman KE, Benner JS, Noren CJ (2000) *J Am Chem Soc* 122:960–961.
34. Aslan FM, Yu Y, Mohr SC, Cantor CR (2005) *Proc Natl Acad Sci USA* 102:8507–8512.
35. Dupuis DE, Guilford WH, Wu J, Warshaw DM (1997) *J Muscle Res Cell Motil* 18:17–30.
36. Mills JP, Qie L, Dao M, Lim CT, Suresh S (2004) *Mech Chem Biosys* 1:169–180.
37. Cecconi C, Shank EA, Bustamante C, Marqusee S (2005) *Science* 309:2057–2060.
38. Song LS, Kim U-S, Wilcoxon J, Schurr JM (1991) *Biopolymers* 31:547–567.
39. Boal D (2002) *Mechanics of the Cell* (Cambridge Univ Press, Cambridge, UK), pp 21–58.
40. Marko JF (1997) *Europhys Lett* 38:183–188.
41. Brau RR, Tarsa PB, Ferrer JM, Lee P, Lang MJ (2006) *Biophys J* 91:1069–1077.
42. Gittes F, Schmidt CF (1998) *Biophys J* 74:A183.
43. Lang MJ, Asbury CL, Shaevitz JW, Block SM (2002) *Biophys J* 83:491–510.